

## Accepted Manuscript

Two new 1D zigzag Hg(II) nanostucture coordination polymers: Sonochemical synthesis, thermal study, crystal structure and Hirshfeld surface analysis

M. Montazerzohori, A. Masoudiasl, Th. Doert

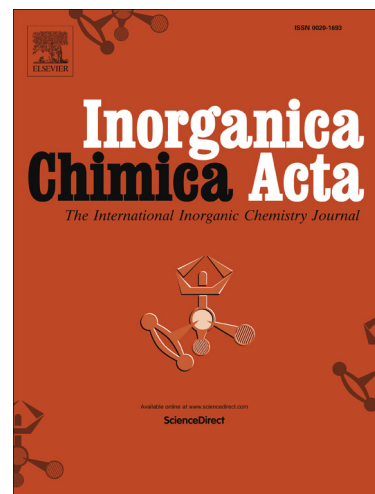
PII: S0020-1693(16)00002-5  
DOI: <http://dx.doi.org/10.1016/j.ica.2016.01.001>  
Reference: ICA 16829

To appear in: *Inorganica Chimica Acta*

Received Date: 7 November 2015  
Revised Date: 1 January 2016  
Accepted Date: 2 January 2016

Please cite this article as: M. Montazerzohori, A. Masoudiasl, Th. Doert, Two new 1D zigzag Hg(II) nanostucture coordination polymers: Sonochemical synthesis, thermal study, crystal structure and Hirshfeld surface analysis, *Inorganica Chimica Acta* (2016), doi: <http://dx.doi.org/10.1016/j.ica.2016.01.001>

This is a PDF file of an unedited manuscript that has been accepted for publication. As a service to our customers we are providing this early version of the manuscript. The manuscript will undergo copyediting, typesetting, and review of the resulting proof before it is published in its final form. Please note that during the production process errors may be discovered which could affect the content, and all legal disclaimers that apply to the journal pertain.



**Two new 1D zigzag Hg(II) nanostructure coordination polymers:  
Sonochemical synthesis, thermal study, crystal structure and Hirshfeld  
surface analysis**

M. Montazerzohori<sup>\*1</sup>, A. Masoudiasl<sup>1</sup>, Th. Doert<sup>2</sup>

<sup>1</sup>Department of Chemistry, Yasouj University, Yasouj 7591874831 Iran.

<sup>2</sup>Department of Chemistry and Food Chemistry, Technische Universität Dresden, 01062 Dresden, Germany.

**\*Corresponding author E-mail: mmzohori@yu.ac.ir**

**ABSTRACT**

Reaction of mercury(II) chloride and bromide with a Schiff base ligand based on isonicotinohydrazide (L) yielded two new 1D zigzag coordination polymers; [Hg( $\mu$ -L)Cl<sub>2</sub>]<sub>n</sub> (**1**) and [Hg( $\mu$ -L)Br<sub>2</sub>]<sub>n</sub> (**2**). The Schiff base ligand and its Hg(II) complexes have been characterized by FT-IR, UV-Vis, <sup>1</sup>H and <sup>13</sup>CNMR spectroscopy. The structures of the complexes were determined by single crystal X-ray diffraction. Structural data show that the two new mercury complexes have similar structures. In both complexes, Hg(II) ion is five-coordinated by three atoms of Schiff base ligand and two halide anions. The ligand (L) acts as N<sub>2</sub>O-donor and connects neighboring Hg ion centers to form infinite 1D zigzag chain. This 1D chain is stabilized as 3D supramolecular network by intermolecular interactions of  $\pi \cdots \pi$  stacking and X-H $\cdots$ Cl (X = N and C) in **1** and C-H $\cdots$  $\pi$ ,  $\pi \cdots \pi$  stacking and X-H $\cdots$ Br (X = N and C) in **2**. Hirshfeld surface analysis and 2D fingerprint plots of asymmetric units of two complexes indicated differences and similarities between crystal packing of compounds. TG/DTG analyses show that compounds **1** and **2** decompose completely during three or four thermal steps, respectively. Nanostructure forms of the titled coordination polymers have been also synthesized by sonochemical method and confirmed by X-ray powder diffraction (XRD), and scanning electron microscopy (SEM).

**Keywords:** Mercury, Coordination, Polymer, X-ray, XRD, Nanostructure, supramolecular.

**1. Introduction**

In the last decades, synthesis and design of coordination polymers have attracted high interest because of their potential applications in adsorption and storage of gases [1,2], sensing [3],

catalysis [4,5], ion exchange [6], magnetism [7] and extraction of metal ions [8]. Crystal engineering of coordination polymers is influenced by judicious design or choice of molecular building blocks and suitable synthetic conditions [9]. Design of organic building blocks having particular functional groups and appropriate coordination sites for specified geometries facilitates rational construction of desired structures and functions by the aid of appropriate metal ions [10-14]. Indeed, the selection of an appropriate organic ligand leads to a particular coordination polymer with intriguing structure and unique properties. On the other hand, the self-assembly processes are sensitive to diverse synthetic conditions and in some cases, change of reaction conditions such as the solvent, pH, counter ion, and temperature for a given set of metal ions and organic ligands can cause various structural topologies [15-19]. Moreover the extraordinary growth of crystal engineering investigations for supramolecular architectures has been accompanied by an increasing interest in the identification and understanding of non-covalent intermolecular interactions. These nonbonding forces control the structures and properties of molecular assemblies such as liquids, molecular crystals and biological molecules [20-22]. Classical and strong hydrogen bonds, and other weaker non-covalent interactions such as C-H...X (X = Hal, O, N),  $\pi$ ... $\pi$  stacking, C-H... $\pi$ , or halogen bonding have attracted some attentions due to stabilization and directionality that they induce to the final structures of crystalline coordination compounds. [23-28]. Among different metal ions, the spherical  $d^{10}$  configuration of Hg(II) is associated with a flexible coordination environment, thus the geometries of the mercury complexes can vary from linear to octahedral or even distorted hexagonal bipyramidal geometries, and severe distortions from ideal coordination polyhedral structure occur easily [29]. In contrast to nano-scale inorganic materials, little attention has been paid to nano-structures of coordination compounds. However, recently, the sonochemical process as a fast, convenient, and economical method has been widely used to produce this type of materials [30-32]. In this synthetic method, molecules undergo a reaction due to the application of powerful ultrasound radiation (10 kHz – 20 MHz) [33]. In the present study, we describe the sonochemical synthesis, spectroscopic studies, thermal study, crystal structures and Hirshfeld surfaces analysis of two novel nanostructured coordination polymers;  $[\text{Hg}(\mu\text{-L})\text{Cl}_2]_n$  (**1**) and  $[\text{Hg}(\mu\text{-L})\text{Br}_2]_n$  (**2**).

## 2.1. Materials and measurements

All reagents used for the syntheses and analysis were commercially available and applied as received. The FT-IR spectra of the compounds were recorded on JASCO-680 spectrophotometer in the range 4000–400  $\text{cm}^{-1}$  using the KBr disk technique. Melting points or decomposition temperatures of the compounds were measured on a Kruss instrument. The  $^1\text{H}$  and  $^{13}\text{C}$  NMR spectra of compounds were recorded by a Bruker DPX FT/NMR-400 spectrometer. A Perkin-Elmer lambda 25 spectrometer has been used for measurement of UV-Visible spectra in dichloromethane solvent in the range of 200–800 nm. X-ray powder diffraction (XRD) measurements were performed using a STOE type STADI-MP-Germany X-ray diffractometer with Cu  $K\alpha$  radiation ( $\lambda = 1.5418 \text{ \AA}$ ). The simulated XRD powder patterns based on single crystal data were prepared using Mercury software [34]. Single crystal diffraction data were collected on a Bruker Kappa APEX II diffractometer with CCD detector (Mo  $K\alpha$  graphite-monochromatic radiation,  $\lambda = 0.71073 \text{ \AA}$ ) controlled by the APEX2 software package [35]. A semi-empirical, absorption correction (multi-scan) was applied with SADABS [36]. The structures were solved by direct methods, SHELXS-97 [37] and refined by full-matrix least-squares refinement cycles on  $F^2$  using SHELXL-97 [38, 39]. Details of crystal data, collection and refinement for the two mercury complexes are listed in Table 1. The record of scanning electron microscopy (SEM) images was carried out by KYKY-EM 3200 field emission scanning electron microscope using Ac voltage of 25 kV. The thermal stabilities for **1** and **2** were investigated by a Perkin-Elmer Pyris model instrument with a heating rate of 10  $^\circ\text{C}/\text{min}$  under nitrogen atmosphere.

## 2.2. Synthesis of N<sup>1</sup>-(4-(dimethylamino)benzylidene)isonicotinohydrazide ligand (L)

Schiff base ligand (L) was prepared according to literature procedure [40-43]. A mixture of 4-(dimethylamino)benzaldehyde (1 mmol, 149.2 mg) and isonicotinic acid hydrazide (1 mmol, 137.1 mg) in ethanol (50 mL) was refluxed for about 24 h. After cooling to room temperature, a yellow precipitate was filtered off and washed twice with ethanol to give the product L as a yellow solid that was stable in air. Yield: 85%. M.p.: 201-203  $^\circ\text{C}$ . UV-Vis,  $\text{CH}_2\text{Cl}_2$  [ $\lambda_{\text{max}}$ , nm]: 258, 361. Selected FT-IR data (KBr,  $\text{cm}^{-1}$ ): 527(w), 582(w), 686(m), 817(s), 1051(m), 1182(m), 1310(m), 1367(s), 1524(s), 1593(s), 1664(s), 2845(m), 2972(w), 3080(w), 3192(m).  $^1\text{H}$ NMR (DMSO- $d_6$ );  $\delta$ : 11.78(s, 1H<sub>c</sub>), 8.77(d, 2H<sub>gg</sub>, J=4.4 Hz), 8.33(s, 1H<sub>d</sub>), 7.81(d, 2H<sub>ff</sub>, J=4.16 Hz), 7.56(d, 2H<sub>cc</sub>, J=7.6 Hz), 6.76(d, 2H<sub>bb</sub>, J=7.6 Hz), 2.99(s, 6H<sub>aa</sub>) ppm.  $^{13}\text{C}$ NMR (DMSO- $d_6$ );  $\delta$ :

161.01(C<sub>7</sub>), 151.67(C<sub>2</sub>), 150.23(C<sub>10,10'</sub>), 145.60(C<sub>6</sub>), 140.80(C<sub>8</sub>), 128.63(C<sub>4,4'</sub>), 123.16(C<sub>5</sub>), 121.43(C<sub>9,9'</sub>), 111.75(C<sub>3,3'</sub>), 39.90(C<sub>1</sub>) ppm.

## 2.2. Synthesis of mercury (II) complexes

### 2.2.1. [Hg(μ-L)Cl<sub>2</sub>]<sub>n</sub> (1)

Crystals of **1** were obtained by slow diffusion in a branched tube [44]. Mercury(II) chloride (101 mg, 0.37 mmol) and Schiff base ligand (L) (100mg, 0.37 mmol) were placed in the main arm of a branched tube and methanol solvent was carefully added to fill the arms. The tube was sealed and the arm containing the reagents immersed in an oil bath at 60 °C while the other arm was kept at ambient temperature. After one week, crystals of **1** were deposited in the cooler arm, which were washed with acetone and ether and analyzed after separation. Yield: 45%. M.p.: 220-222°C. UV-Vis, CH<sub>2</sub>Cl<sub>2</sub> [ $\lambda_{\max}$ , nm]: 256, 358. Selected FT-IR data (KBr, cm<sup>-1</sup>): 451(w), 509(w), 572(w), 692(s), 804(m), 1061(m), 1180(s), 1376(s), 1533(m), 1585(s), 1639(s), 2821(m), 2902(w), 3081(w), 3263(m). <sup>1</sup>HNMR (DMSO-d<sub>6</sub>);  $\delta$ : 11.81(s, 1H<sub>c</sub>), 8.78(d, 2H<sub>gg'</sub>), 8.33(s, 1H<sub>d</sub>), 7.86(d, 2H<sub>ff</sub>, J=4.00 Hz), 7.56(d, 2H<sub>cc'</sub>, J=7.6 Hz), 6.76(d, 2H<sub>bb'</sub>, J=7.6 Hz), 2.99(s, 6H<sub>aa'</sub>) ppm. <sup>13</sup>CNMR (DMSO-d<sub>6</sub>);  $\delta$ : 160.85(C<sub>7</sub>), 151.69(C<sub>2</sub>), 149.95(C<sub>10,10'</sub>), 145.61(C<sub>6</sub>), 141.31(C<sub>8</sub>), 128.66(C<sub>4,4'</sub>), 123.63(C<sub>5</sub>), 121.74(C<sub>9,9'</sub>), 111.76(C<sub>3,3'</sub>), 39.87(C<sub>1</sub>) ppm.

### 2.2.1. [Hg(μ-L)Br<sub>2</sub>]<sub>n</sub> (2)

Crystals of **2** were prepared by a similar manner as complex **1** except that mercury(II) chloride was replaced by mercury(II) bromide. Yield: 53%. M.p.: 246-248°C. UV-Vis, CH<sub>2</sub>Cl<sub>2</sub> [ $\lambda_{\max}$ , nm]: 261, 353. Selected FT-IR data (KBr, cm<sup>-1</sup>): 453(w), 509(w), 559(w), 692(s), 804(m), 1061(m), 1189(s), 1375(s), 1533(m), 1583(s), 1633(s), 2821(m), 2908(w), 3077(w), 3272(m). <sup>1</sup>HNMR (DMSO-d<sub>6</sub>);  $\delta$ : 11.80(s, 1H<sub>c</sub>), 8.77(d, 2H<sub>gg'</sub>, J=6.00 Hz), 8.33(s, 1H<sub>d</sub>), 7.85(d, 2H<sub>ff</sub>, J=7.60 Hz), 7.56(d, 2H<sub>cc'</sub>, J=8.80 Hz), 6.60(d, 2H<sub>bb'</sub>, J=8.80 Hz), 2.99(s, 6H<sub>aa'</sub>) ppm. <sup>13</sup>CNMR (DMSO-d<sub>6</sub>);  $\delta$ : 160.75(C<sub>7</sub>), 151.69(C<sub>2</sub>), 150.04(C<sub>10,10'</sub>), 145.60(C<sub>6</sub>), 141.28(C<sub>8</sub>), 128.65(C<sub>4,4'</sub>), 123.60(C<sub>5</sub>), 121.74(C<sub>9,9'</sub>), 111.75(C<sub>3,3'</sub>), 39.89(C<sub>1</sub>) ppm..

## 2.3. Synthesis of nanostructure mercury compounds [Hg(μ-L)X<sub>2</sub>]<sub>n</sub> (X = Cl for **1** and X = Br for **2**)

For the synthesis of nanostructure mercury(II) complexes, an ethanol/dichloromethane (10:1, v/v) solution of Schiff base ligand (1 mmol) was positioned under ultrasonic irradiation. Then, an ethanolic solution of mercury(II) halide (1 mmol) was drop wisely added. The reaction mixture was kept in the ultrasonic bath for about 60 min. The obtained precipitates were filtered and washed with ethanol several times and then dried at 70 °C.

## 2.4. Hirshfeld surfaces calculations

Molecular Hirshfeld surface analyses were carried out by using the CrystalExplorer computer program [45]. Hirshfeld surfaces are mapped using the normalized contact distance ( $d_{norm}$ ), which is calculated using the following equation:

$$d_{norm} = \frac{d_i - r_i^{vdw}}{r_i^{vdw}} + \frac{d_e - r_e^{vdw}}{r_e^{vdw}}$$

Where  $d_e$  is the distance from the Hirshfeld surface to the nearest atom outside the surface,  $d_i$  is the distance from the Hirshfeld surface to the nearest atom inside the surface and  $d_{norm}$  is defined in terms of  $d_e$  and  $d_i$  and the van der Waals (vdW) radii of atoms. Three-dimensional (3D) Hirshfeld surface maps are generated with  $d_{norm}$  using a red–white–blue color scheme, indicating shorter contacts, vdW contacts, and longer contacts, respectively, and two dimensional (2D) fingerprint plots generated using  $d_e$  and  $d_i$ .

## 3. Results and discussion

### 3.1. Spectroscopic studies

A schematic representation of Schiff base ligand (L) and its coordination mode to Hg(II) center is illustrated in Scheme 1. Data related to FT-IR, NMR and UV-Vis spectra of ligand and its mercury(II) complexes have been described in Section 2. In the FT-IR spectrum of the ligand, the absorption peak around 3192  $\text{cm}^{-1}$  is attributed to N–H stretching frequency. After complexation, this absorption peak shifted to higher frequencies (3263  $\text{cm}^{-1}$  in **1** and 3272  $\text{cm}^{-1}$  in **2**). The C=O stretching frequency of ligand appeared around 1664  $\text{cm}^{-1}$  as sharp peak shifts to a lower wavenumbers in the spectra of complexes (1639  $\text{cm}^{-1}$  in **1** and 1633  $\text{cm}^{-1}$  in **2**). Also the absorption peak at 1593  $\text{cm}^{-1}$  related to C=N stretching vibration of ligand shifts to lower

frequencies in the complexes spectra ( $1585\text{ cm}^{-1}$  in **1** and  $1583\text{ cm}^{-1}$  in **2**). These signal shifts confirm the participation of the imine nitrogen and carbonyl oxygen of the ligand in binding to the mercury center. Moreover, the presence of new peaks in the IR spectra of the synthesized complexes at  $450 - 510\text{ cm}^{-1}$  can be assigned to  $\nu(\text{M-N})$  vibrations that may be as an evidence for the coordination of nitrogen atom to the metal center [46].

The UV-Visible spectra of free ligand exhibits two bands, one as a shoulder at 258 nm assigned to  $\pi \rightarrow \pi^*$  transitions due to  $\pi$ -system of pyridine and phenyl rings and carbonyl and azomethine bonds and the second one as intense bond at 361 nm assigned to  $n \rightarrow \pi^*$  transitions of C=O and C=N groups [47]. The red and blue shifts of the these bands in the complexes spectra with respect to the free ligand indicate the coordination of the ligand to the Hg(II) ion. In continuation, NMR spectra of ligand and its mercury complexes were also recorded to confirm the suggested structures. In the ligand spectrum, imidic hydrogen ( $\text{H}_e$ ) appears as a singlet peak at 11.78 ppm. Olefinic hydrogen of  $\text{H}_d$  appears as a singlet signal at 8.33 ppm. Aromatic hydrogens of  $\text{H}_{gg'}$ ,  $\text{H}_{ff'}$ ,  $\text{H}_{cc'}$  and  $\text{H}_{bb'}$  are found as doublet signals at 8.77, 7.81, 7.56 and 6.76 ppm respectively. Finally, aliphatic hydrogens of 6  $\text{H}_{aa'}$  resonate at 2.99 ppm. After coordination, chemical shifts of the hydrogens are unchanged or downfielded. In  $^{13}\text{C}$  NMR spectrum of ligand, carbon signals of ( $\text{C}_7$ ), ( $\text{C}_2$ ), ( $\text{C}_{10,10'}$ ), ( $\text{C}_6$ ), ( $\text{C}_8$ ), ( $\text{C}_{4,4'}$ ), ( $\text{C}_3$ ), ( $\text{C}_{9,9'}$ ), ( $\text{C}_{3,3'}$ ) and ( $\text{C}_1$ ) appear at 161.01, 151.67, 150.23, 145.60, 140.80, 128.63, 123.16, 121.43, 111.75 and 39.90 ppm respectively. After binding of ligand to mercury center, the carbon signals are appeared as downfielded or upfielded signals as detailed in experimental section.

### Scheme 1

## 3.2. Crystal structures description

Crystal structure of ligand has been previously reported [40-43]. Tables of 1 and 2 show the X-ray structure determination details, selected bond lengths and bond angles of the compounds (**1** and **2**), respectively. The intermolecular interactions of compounds are listed in Table 3.

### 3.2.1. $[\text{Hg}(\mu\text{-L})\text{Cl}_2]_n$ (**1**)

Single-crystal X-ray diffraction analysis revealed that **1** crystallizes in the orthorhombic space group  $P_{bca}$ . Crystal structure and asymmetric unit of **1** are shown in Fig. 1. The asymmetric unit is composed of one Hg(II) ion, one Schiff base ligand (L), and two chloride anions. The Hg(II) ion is five-coordinated by three atoms of Schiff base ligand (imine nitrogen, pyridine nitrogen and carbonyl oxygen) and two Cl atoms. The Schiff base ligand (L) acts as  $N_2O$ -donor (Scheme 1), and connects to neighboring Hg centers to form an infinite 1D zigzag chain (Fig. 3). According to equation defined by Addison et al [48] for five coordinated compounds, the value of  $\tau_5$  parameter is 0.24, indicating a distorted square pyramidal (SP) geometry for the mercury (II) center. In this SP coordination, the equatorial plane contains two nitrogen atoms of two distinct Schiff base ligands (imine nitrogen from one and pyridine nitrogen from other) and two terminal chloride anions and the apical position is occupied by carbonyl oxygen atom of ligand. The Hg, Cl1 and Cl2 atoms lie out of the mean plane defined by N1N3HgCl1Cl2 by a distance of 0.154, 0.674 and 0.780 Å to the opposite side of apical oxygen (O1), while the pyridine nitrogen(N1) and imine nitrogen(N3) are displaced toward apical position by distances of 0.867 and 0.740 Å, respectively. The Hg–N<sub>pyridin</sub> bond length (2.547 Å) is significantly shorter than the Hg–N<sub>imine</sub> bond length (2.80 Å), and the Hg–O<sub>carbonyl</sub> bond length is shorter than these two bonds. In a reported pyrrole hydrazone mercury complex [49], this order changes as following: Hg–N<sub>imine</sub> < Hg–N<sub>pyridin</sub> < Hg–O<sub>carbonyl</sub>. The average Hg–Cl distance (2.354 Å) is comparable with its average value in mercury complexes containing HgN<sub>2</sub>OC<sub>2</sub> chromophore [49, 50]. The angles around the Hg center is ranging from 62.16(4)° to 151.76(16)°. The Schiff base ligand form a five-membered chelate ring with bite angle of about 62.16° that is close to its value (60.35°) in pyrrole hydrazone mercury complex [49].

As shown in Fig. 3, the Hg(II) atoms are connected through bridging Schiff base ligand(L) that results in 1D zigzag chain. The crystal packing analyses shows that 1D chains are further arranged in the crystal lattice by  $\pi \cdots \pi$  stacking and X–H $\cdots$ Cl (X = N and C) intermolecular interactions. The Cl1 atom participates in hydrogen bonding with hydrogen atom (H14C) of the methyl group of substituent on phenyl ring. This C–H $\cdots$ Cl non-covalent interaction leads to 2D expansion of crystal network (Fig. 4(left)). The polymeric chains are also embraced through intermolecular  $\pi \cdots \pi$  stacking interactions between pyridine rings of Schiff base ligand with a centroid-to-centroid distance of 3.733 Å and symmetry code (-1/2+x, y, 1/2-z) for C<sub>g</sub>1 $\cdots$ C<sub>g</sub>1 (C<sub>g</sub>1: N1, C1, C2, C3, C4, C5). These chains are further embraced through intermolecular N–H

···Cl hydrogen bonds between Cl2 atom and amide hydrogen (H2A) of Schiff base ligand. These two last interactions induce consecutive layers of polymeric chains (Fig. 4(right)). The dihedral angle between planes of two adjacent polymeric chains is 10.3° indicating these chains are almost parallel.

### 3.2.2. [Hg( $\mu$ -L)Br<sub>2</sub>]<sub>n</sub> (**2**)

X-ray single crystal diffraction analysis and vibrational spectroscopic studies reveal that the two mercury(II) coordination polymers have similar structures. The asymmetric unit of **2** is shown in Fig. 2. This compound consists of 1D polymeric chains of  $\mu$ -L-connected square pyramidal (SP) complexes (Fig. 3). In the distorted square pyramidal geometry ( $\tau_5 = 0.07$ ) of the mercury(II) center, the equatorial positions are occupied by pyridine nitrogen(N1), imine nitrogen(N3) and two bromide anions (Br1 and Br2) while the carbonyl oxygen atom (O1) is at the apical position. The distance of Hg1 from the mean plane defined by N1N3HgBr1Br2 is 0.056 Å. The bonds of the central atom to the coordinating ligand atoms have almost identical lengths ( $\Delta\text{Hg-N}_{\text{pyridine}} = 0.005$  Å,  $\Delta\text{Hg-N}_{\text{imine}} = 0.04$  Å and  $\Delta\text{Hg-O}_{\text{carbonyl}} = 0.011$  Å). In both complexes, the Hg–N<sub>imine</sub> bond distance is longer than the range previously reported for five-coordinated mercury complexes involving ligation by imine nitrogen atom [49-52]. However, Hg–N bonds longer than 2.76 Å have been reported in several Hg(II) compounds [53-54].

In the crystal packing of **2**, distinct C–H··· $\pi$  interactions are accompanied by  $\pi$ - $\pi$  stacking and X–H···Br (X = N and C) interactions (Table 3). Edge-to-face C14–H14c···Cg2 (Cg2: C8-C13) interactions are formed between hydrogen atom (H14C) of the methyl group from one polymeric chain with phenyl ring from the next polymeric chain. These interactions expand the chains to a 2D network (Fig. 5(left)). Also, these layers of polymeric chains are embraced inside this 2D network through  $\pi$ - $\pi$  stacking interactions and X–H···Br hydrogen bonds. Intermolecular  $\pi$ ··· $\pi$  stacking interactions exhibit two types of pairwise embrace. One embrace involves  $\pi$ ··· $\pi$  interactions between pyridine rings, while the other involves  $\pi$ ··· $\pi$  interactions between phenyl rings. Interacting pyridine planes [Cg1···Cg1 (Cg1: N1, C1, C2, C3, C4, C5 and symmetry code: -1/2+x, 1/2-y, z)] are approximately parallel (dihedral angle: 2.678°) with a centroid–centroid distance of 3.769 Å. The interaction between phenyl rings [Cg2···Cg2, (Cg2: C8-C13 and symmetry code: 1-x, 1-y, z)] is weaker with a centroid–centroid distance of 3.919 Å and a dihedral angle of 6.824°, respectively. On the other hand, adjacent layers are further embraced by

formation of X–H···Br hydrogen bonds. Br<sub>2</sub> atom from one polymeric chain interacts with amide hydrogen (H<sub>2a</sub>) and aromatic hydrogen (H<sub>5</sub>) on pyridine ring from its neighbor chain by the formation of N–H···Br and C–H···Br hydrogen bonds, respectively (Table 3). These intermolecular interactions expand 1D chains to a 3D supramolecular architecture (Fig. 5(right)). In this complex, the dihedral angle between two adjacent layers is 23.32°.

**Table 1**

**Table 2**

**Table 3**

**Fig. 1**

**Fig. 2**

**Fig. 3**

**Fig. 4**

**Fig. 5**

### 3.3. Molecular Hirshfeld surfaces

The Hirshfeld surface analyses of two Hg(II) coordination polymers have been performed on their asymmetric unit. The Hirshfeld surfaces mapped over  $d_{\text{norm}}$  (-0.335 to 1.229 Å) are displayed in Figs. 6 and 7 as transparent to permit visualization of the respective molecules. The most obvious red spots on the  $d_{\text{norm}}$  surface of both complexes (one near to the Hg atom and another on the pyridine nitrogen atom) are due to the Hg···N interactions. Two remaining visible red regions on  $d_{\text{norm}}$  surface of **1** refer to X–H···Cl (X = N and C) interactions. The  $d_{\text{norm}}$  surface of **2** contains several large red regions. Some of them are invisible on  $d_{\text{norm}}$  surface of **1**. Two doublet red spots are due to H···C contacts (C–H··· $\pi$  interactions). Also, H···H interactions are observed as two small light red spots around the hydrogen atoms on the phenyl rings. The interactions of Br atom with various hydrogen atoms (H···Br interactions) are visible as small light red regions. The 2D fingerprint plots are used for identification and separation of intermolecular interactions and relative contribution of these interactions can be obtained from the area of the surfaces [55]. The 2D fingerprint plots of compounds, displayed by the standard view, are shown in Fig. 8. The comparison of the relative contributions of different interactions

(Fig. 9) indicates the more or less identical contribution of interactions in these two mercury complexes due to their structural similarity.  $H\cdots H$  (29.4%) and  $X-H\cdots Br$  (29.7%) contacts have the highest share of Hirshfeld surface in **1** and **2**, respectively.  $H\cdots H$  interactions appeared as a very distinct spike on the diagonal of the plots. They have the lowest value of  $d_e + d_i$  in both complexes ( $\approx 2.2$  Å in **1** and  $2.1$  Å in **2**). The interaction of the hydrogens with the coordinated halogens ( $H\cdots Halogen$  interaction) comprises a high share of the Hirshfeld surface (28.8% in **1** and 29.7% in **2**) and appear as wings on the top left ( $H\cdots halogen$ ) and bottom right ( $halogen\cdots H$ ) of the 2D fingerprint plots. These contacts are due to  $N-H\cdots Halogen$  and  $C-H\cdots Halogen$  intermolecular interactions.  $C\cdots H/H\cdots C$  contacts ( $C-H\cdots \pi$  interactions) comprise 15.8% and 14.3% of the surface for each molecule in complex **1** and **2**, respectively. In spite of the high share of  $C\cdots H/H\cdots C$  contacts in **1**, no significant  $C-H\cdots \pi$  interactions are observed in this compound, while these interactions are observed as doublet distinct red spots on the  $d_{norm}$  surface of **2**. These interactions manifest as two weak spikes beside  $H\cdots Cl$  interactions in the fingerprint plot of **1**, while they are visible as two partly flat spikes in the plot of **2**.  $C\cdots C$  contacts ( $\pi$ -Stacking interactions) appear in the central region of the plots and they comprise area fractions of 4.8% and 5.3% in **1** and **2** complexes, respectively.

**Fig. 6**

**Fig. 7**

**Fig. 8**

**Fig. 9**

### 3.4. Thermal analyses

The thermal stability of the coordination polymers were investigated based on thermogravimetric method at a heating rate of  $10$  °C/min under nitrogen atmosphere. Figures of 10 and 11 present the TG/DTG plots of the mercury complexes. The thermal analyses data including temperature range, mass loss (%) and kinetic activation parameters of thermal decomposition steps obtained from the TG/DTG plots are listed in Table 4. The thermal decomposition processes of **1** and **2** occur in three and four thermal steps, respectively. In both complexes, the first thermal step is related to the removal of one  $CH_3$  group. The second thermal degradation step of **1** happens in

the range of 222–395 °C and corresponds to the loss of nonmetallic parts (Schiff base ligand and chloride anions), accompanied by a weight loss of 61.46% (calculated: 60.0%). The mercury atom is lost in the final thermal step. Compound **2** loses the pyridine and the substituted phenyl ring in the second step; the residual parts of the ligand and one of the coordinated bromide anions in third step and Hg-Br fragment in last step without final residue. Moreover, the kinetic and thermodynamic parameters for the decomposition processes of Hg(II) coordination polymers including the activation energy ( $E^*$ ), the enthalpy of activation ( $\Delta H^*$ ), the entropy of activation ( $\Delta S^*$ ) and the free energy of activation ( $\Delta G^*$ ) were investigated graphically by using the Coats–Redfern relation [56], the obtained data are tabulated as Table 5. The positive values of activation energies ( $E^*$ ) in the range of 37.87–588.58 kJ·mol<sup>-1</sup> for the thermal decomposition steps reveals the high stability of the compounds [57, 58]. The higher activation energy of the first decomposition step for **1** suggests its enhanced thermal stability against decomposition as compared with **2**. Positive values of the activation entropies ( $\Delta S^*$ ) at the first thermal steps of both complexes may indicate the dissociation character of the decomposition [57, 59]. The negative values of  $\Delta S^*$  for other decomposition steps indicate more ordered activated complex than the reactants or a slower reaction rate than normal degradation processes. The positive values of the enthalpy of activation ( $\Delta H^*$ ) in the range of 31.19–584.55 kJ·mol<sup>-1</sup> indicates the endothermic nature of all thermal decomposition steps. Also, the positive values of the Gibbs free energy of activation ( $\Delta G^*$ ) reflects the non-spontaneous nature of thermal decomposition processes. On the other hand, the significant increase of values of  $\Delta G^*$  for consecutive decomposition steps of both compounds is due to the increase of the values of  $T\Delta S^*$  which overcome the values of  $\Delta H^*$  [59].

**Table 4**

**Fig. 10**

**Fig. 11**

### 3.5. Characterization of nanostructured mercury complexes

The experimental XRD pattern of both compounds prepared by the sonochemical process in comparison with simulated ones on the basis of the single crystal X-ray analysis are shown in Fig. 12. All major peaks of sonochemically prepared compounds match well with those of the simulated PXRD, indicating their crystalline phase purity. The significant broadening of the peaks of the sonochemically synthesized compounds indicates that the particles are of nanometer

dimensions. The average size of particles was estimated from Scherer's equation ( $D = \frac{k\lambda}{\beta \cos \theta}$ , where  $D$  is the average grain size,  $K$  is Scherrer's constant (0.891),  $\lambda$  is the X-ray wavelength (0.15405 nm),  $\theta$  and  $\beta$  are the diffraction angle and full-width at half maximum of an observed peak, respectively). The obtained values for **1** and **2** are 40 and 39 nm, respectively. SEM images have been used for investigation of morphology and size of the coordination polymers prepared under sonochemical conditions. Fig. 13 illustrates the SEM images of compounds **1** and **2**. These images show spherical morphology with diameters of nano-dimension. In both compounds, the particles are agglomerated and particle size distribution is almost homogeneous.

**Fig. 12**

**Fig. 13**

#### 4. Conclusion

Two new one dimensional zigzag Hg(II) coordination polymers based on N'-(4-(dimethylamino)benzylidene)isonicotinohydrazide Schiff base ligand (L) were prepared and identified by different spectroscopic techniques and X-ray crystallography. Structural data showed that two complexes have similar structure; both crystallize in the orthorhombic system. In both complexes, the Hg(II) ion is five-coordinated by three atoms of the Schiff base ligand and two halide anions. The coordination geometry of the complex is a distorted square pyramidal based on  $\tau_5$  parameter (0.24 for **1** and 0.07 for **2**). The Schiff base ligand (L) acts as N<sub>2</sub>O-donor and connects to neighboring Hg centers to form infinite 1D zigzag chain. The crystal packing analysis of two complexes revealed that 3D supramolecular architectures can produce from one dimensional coordination chains through  $\pi \cdots \pi$  stacking and X-H $\cdots$ Cl (X = N and C) intermolecular interactions in **1** and C-H $\cdots$  $\pi$ ,  $\pi \cdots \pi$  stacking and X-H $\cdots$ Br (X = N and C) interactions in **2**. Hirshfeld surface analyses exhibited effective role of C-H $\cdots$  $\pi$  and H $\cdots$ H contacts in crystal packing of **2**. The 2D fingerprint plots indicate the more or less identical contributions of interactions in the complexes arising from their structural similarity. TG/DTG diagrams showed that the thermal decomposition process of **1** and **2** occurs in three and four thermal steps without final residue, respectively. The sonochemical process, as a simple, low cost and environmentally friendly approach, has been used for synthesis of nanostructure coordination polymers. Comparing the XRD pattern of two sonochemically prepared compounds

with the simulated XRD pattern from single crystal X-ray analysis indicates that the compounds obtained by two methods are identical except in particle sizes.

**Supplementary information:** CCDC 1435591 and 1435593 are corresponded to the supplementary crystallographic data for this paper. These data are available free of charge at <http://www.ccdc.cam.ac.uk/conts/retrieving.html>.

**Acknowledgement:** Partial support of this work by Yasouj University is acknowledged.

## References

- [1] M. E. Kosal, J. -H. Chou, S. R. Wilson, K. S. Suslick, *Nat. Mater.* 1 (2002) 118-121.
- [2] F. Deng, W. Ding, Z. Peng, L. Li, X. Wang, X. Wan, L. Cheng, M. Li, *Journal of Alloys and Compounds* 647 (2015) 1111-1120.
- [3] J. Yang, B. Zhou, J. Yao, X. -Q. Jiang, *Biosens. Bioelectron.*, 67, (2015) 66-72.
- [4] F. -X. Bu, M. Hu, L. Xu, Q. Meng, G. -Y. Mao, D. -M. Jiang, J. -S. Jiang, *Chem. Commun.*, 50 (2014) 8543-8546.
- [5] M. Y. Masoomi, S. Beheshti, A. Morsali, *Cryst. Growth Des.*, 15 (2015) 2533–2538.
- [6] K. Ooi, Y. Tasaki-Handa, Y. Abe, A. Wakisaka, *Dalton Trans.*, 43 (2014) 4807-4812.
- [7] G. Zhuang, W. Chen, J. Zheng, H. Yu, J. Wang, *J. Solid State Chem.*, 192, (2012) 284-288.
- [8] E. Tahmasebi, M Y Masoomi, Y. Yamini, A. Morsali, *Inorg. Chem.*, 54 (2015) 425–433.
- [9] M. -C. Hong, L. Chen, design and construction of coordination polymers, Wiley, New Jersey, 2009.
- [10] S. R. Batten, R. Robson, *Angew. Chem., Int. Ed.* 37 (1998) 1461–1494.
- [11] L. Carlucci, G. Ciani, D. M. Proserpio, *Coord. Chem. Rev.* 246 (2003) 247–289.
- [12] O. M. Yaghi, M. O’Keeffe, N. W. Ockwig,; H. K. Chae, M. Eddaoudi,; J. Kim, *Nature* 423 (2003) 705–714.
- [13] S. Kitagawa, R. Kitaura, S. I. Noro, *Angew. Chem., Int. Ed.* 43 (2004) 2334–2375.

- [14] M. Y. Masoomi, A. Morsali, *RSC Adv.*, 3 (2013) 19191-19218.
- [15] L. -S. Long, *CrystEngComm.*, 12 (2010) 1354.
- [16] S. Masaoka, D. Tanaka, Y. Nakanishi, S. Kitagawa, *Angew. Chem. Int. Ed.* 43 (2004) 2530.
- [17] X.-Y. Wang, L. Wang, Z. -M. Wang, S. Gao, *J. Am. Chem. Soc.*, 128 (2006) 674.
- [18] J. L. Sague, M. Meuwly, K. M. Fromm, *CrystEngComm*, **10** (2008) 1542-1549.
- [19] M. Y. Masoomi, A. Morsali, P. C. Junk, *RSC Adv.*, 4 (2014) 47894-47898.
- [20] A. D. Buckingham, P. Fowler and J. M. Hutson, *Chem. Rev.*, 88(1988) 963.
- [21] G. Chalasinski, M. M. Szczesniak, *Chem. Rev.*, 100 (2000) 4227.
- [22] E. A. Meyer, R. K. Castellano, F. Diederich, *Angew. Chem. Int. Ed.*, 42 (2003) 1210.
- [23] L. J. Prins, D. N. Reinhoudt, P. Timmerman, *Angew. Chem., Int. Ed.*, 40 (2001) 2382–2426.
- [24] G. R. Desiraju, T. Steiner, *The Weak Hydrogen Bond: In Structural Chemistry and Biology*; Desiraju, G. R., Steiner, T., Eds.; Oxford University Press Inc.: New York, 1999.
- [25] T. Steiner, *Angew. Chem., Int. Ed.*, 41 (2002) 48–76.
- [26] C. Janiak, *J. Chem. Soc., Dalton Trans.* (2000) 3885–3896.
- [27] M. Nishio, *CrystEngComm* 6 (2004) 130–158.
- [28] P. Metrangolo, G. Resnati, *Science* 321 (2008) 918–919.
- [29] A. Morsali, M. Y. Masoomi, *Coord. Chem. Rev.*, 253 (2009) 1882–1905.
- [30] M. Montazerzohori, S. Mojahedi Jahromi, A. Masoudiasl, P. McArdle, *Spectrochim. Acta, Part A*, 138 (2015) 517–528.
- [31] V. Safarifard, A. Morsali, *Coord. Chem. Rev.*, 292 (2015) 1–14.
- [32] M. Y. Masoomi, A. Morsali, *Coord. Chem. Rev.*, 256 (2012) 2921– 2943.
- [33] K. S. Suslick, S. -B. Choe, A. A. Cichowlas, M. W. Grinstaff, *Nature* 353 (1991) 414–416.
- [34] MERCURY 1.4.1, Copyright Cambridge Crystallographic Data Centre, 12 Union Road, Cambridge, CB2 1EZ, UK, 2001–2005.
- [35] Apex Suite (V. 2014.2), Bruker AXS Inc., Madison, WI, USA, **2014**.
- [36] SADABS. G. M. Sheldrick, Bruker AXS Area Detector Scaling and Absorption Correction, Göttingen, Germany, **2008**.

- [37] SHELXS-97, *Program for the Solution of Crystal Structures*, G. M. Sheldrick, Göttingen, Germany **1997**.
- [38] SHELXL-97, *Program for the Refinement of Crystal Structures*, G. M. Sheldrick, Göttingen, Germany **1997**.
- [39] SHELXLE: A Qt graphical user interface for Shelxl, C. B. Hübschle, G. M. Sheldrick, B. Dittrich, *J. Appl. Cryst.* 44 (2011) 1281–1284.
- [40] H. -K. Fun, K. Sivakumar, Z. -L. Lu, C. -Y. Duan, Y. -P. Tian, X. -Z. You, *Acta Cryst. C*, 52 (1996) 1505-1507.
- [41] M. G. Tsintsadze, G. G. Aleksandrov, V. S. Sergienko, G. V. Tsintsadze, *Kristallografiya*, 41(1996) 791.
- [42] D. -S. Yang, *J. Chem. Cryst.*, 37 (2007) 343-348.
- [43] H. Sahebalzamani, N. Khaligh, S. Ghammamy, F. Salimi, K. Mehrani, *Molecules*, 16 (2011) 7715-7723.
- [44] M. Y. Masoomi, M. Bagheri, A. Morsali *Inorg. Chem.*, 54(2015) 11269-11275.
- [45] S. K. Wolff, D. J. Grimwood, J. J. McKinnon, M. J. Turner, D. Jayatilaka, M. A. Spackman, *CrystalExplorer*, University of Western Australia, 2012.
- [46] D. X. West, A. A. Nassar, *Trans. Met. Chem.* 24 (1999) 617–621.
- [47] R. L. Carlin, F. Ann Walker, *J. Am. Chem. Soc.* 87 (1965) 2128-2133.
- [48] A. W. Addison, T. N. Rao, J. Reedijk, J. V. Rijn, G. C. Verschoor, *J. Chem. Soc., Dalton Trans.* (1984) 1349.
- [49] J. Wang, B. Liu, B. Yang, *CrystEngComm*, 13 (2011) 7086.
- [50] S. Saha, P. Mahato, Upendar Reddy G, E. Suresh, A. Chakrabarty, M. Baidya, S. K. Ghosh, A. Das, *Inorg. Chem.* 51 (2012) 336.
- [51] S. Satapathi, S. Choubey, S. Das, K. Bhar, R. Ghosh, P. Mitra, B. K. Ghosh, *J. Chem. Cryst.* 42 (2012) 1062.
- [52] A. A. Khandar, V. T. Yilmaz, F. Costantino, S. Gumus, S. A. Hosseini-Yazdi, G. Mahmoudi, *Inorg. Chim. Acta* 394 (2013) 36–44.
- [53] E. Lopez-Torres, M. A. Mendiola, *Inorg. Chim. Acta* 363 (2010) 1275.

- [54] M. Montazerzohori, S.A. Musavi, A. Hojjati, A. Assoud, *Spectrochim. Acta A* 147 (2015) 139–150.
- [55] M. A. Spackman, P. G. Byrom, *Chem. Phys. Lett.*, 1997, 267, 215–220.
- [56] A. W. Coats, J. P. Redfern, *Nature* 20 (1964) 68.
- [57] M. Montazerzohori, S. A. Musavi, A. Naghiha, M. MontazerZohour, *Spectrochim. Acta A* 129 (2014) 382–391
- [58] T. Taakeyama, F. X. Quinn, *Thermal Analysis Fundamentals and Applications to Polymer Science*, John Wiley and Sons, Chichester, 1994.
- [59] S. S. Kandil, G. B. El-Hefnawy, E. A. Baker, *Thermochim. Acta* 414 (2004) 105–113.

**Scheme, Figures and table captions:**

**Scheme 1.** Atom numbering representation of Schiff base ligand and its coordination mode to metal center.

**Fig. 1.** Part of crystal structure of  $[\text{Hg}(\mu\text{-L})\text{Cl}_2]_n$  (**1**). Hydrogen atoms are omitted for clarity. (Symmetry transformations used to generate equivalent atoms: #1:  $-x+1, y+1/2, -z+1/2$  and #2:  $-x+1, y-1/2, -z+1/2$ ).

**Fig. 2.** Asymmetric unit of  $[\text{Hg}(\mu\text{-L})\text{Br}_2]_n$  (**2**), hydrogen atoms are omitted for clarity.

**Fig. 3.** Polymeric 1D zigzag chain in [top]  $[\text{Hg}(\mu\text{-L})\text{Cl}_2]_n$  (**1**) and [bottom]  $[\text{Hg}(\mu\text{-L})\text{Br}_2]_n$  (**2**).

**Fig. 4.** [left] View of 2D network induced by  $\text{C-H}\cdots\text{Cl}$  interactions and [right] embraced chains by  $\pi\cdots\pi$  stacking and  $\text{N-H}\cdots\text{Cl}$  interactions (green dotted lines:  $\pi\cdots\pi$  stacking and black dotted lines:  $\text{N-H}\cdots\text{Cl}$  interactions) in crystal packing of **1**.

**Fig. 5.** [left] View of 2D network induced by  $\text{C-H}\cdots\pi$  interactions and [right] View of 3D supramolecular network induced by intermolecular interactions in **2**.

**Fig. 6.** The Hirshfeld surface of  $[\text{Hg}(\mu\text{-L})\text{Cl}_2]_n$  (**1**) mapped over  $d_{\text{norm}}$ .

**Fig. 7.** The Hirshfeld surface of  $[\text{Hg}(\mu\text{-L})\text{Br}_2]_n$  (**2**) mapped over  $d_{\text{norm}}$  from two different views.

**Fig. 8.** 2D fingerprint plots of [left]  $[\text{Hg}(\mu\text{-L})\text{Cl}_2]_n$  (**1**) and [right]  $[\text{Hg}(\mu\text{-L})\text{Br}_2]_n$  (**2**).

**Fig. 9.** Relative contributions to the Hirshfeld surface area for the various intermolecular contacts in two complexes.

**Fig. 10.** The TG diagrams of both Hg(II) coordination polymers.

**Fig. 11.** The DTG diagrams of both Hg(II) coordination polymers.

**Fig. 12.** XRD patterns of simulated pattern based on single crystal data and nanostructure prepared by sonochemical process of [A]  $[\text{Hg}(\mu\text{-L})\text{Cl}_2]_n$  (**1**) and [B]  $[\text{Hg}(\mu\text{-L})\text{Br}_2]_n$  (**2**).

**Fig. 13.** SEM images of coordination polymers **1** (A) and **2** (B) prepared by sonochemical process.

**Table 1**

Crystal data and structure refinement for  $[\text{Hg}(\mu\text{-L})\text{Cl}_2]_n$  (**1**), and  $[\text{Hg}(\mu\text{-L})\text{Br}_2]_n$  (**2**)

**Table 2**

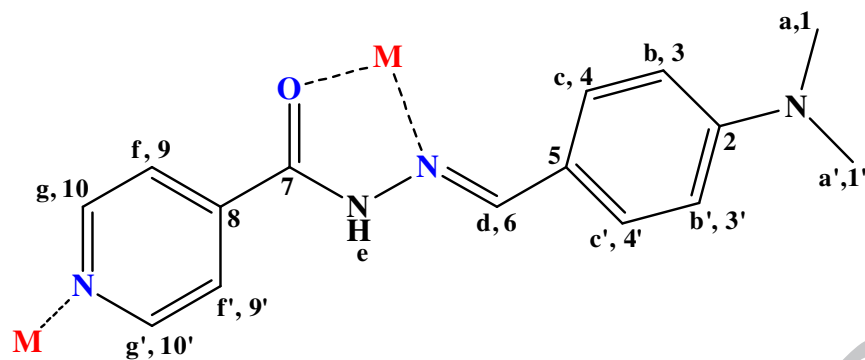
Bond lengths (Å) and angles (°) for  $[\text{Hg}(\mu\text{-L})\text{Cl}_2]_n$  (**1**) and  $[\text{Hg}(\mu\text{-L})\text{Br}_2]_n$  (**2**)

**Table 3**

Intermolecular interactions in crystal packing of  $[\text{Hg}(\mu\text{-L})\text{Cl}_2]_n$  (**1**) and  $[\text{Hg}(\mu\text{-L})\text{Br}_2]_n$  (**2**)

**Table 4**

Thermal analysis data including temperature range, mass loss and thermodynamic activation parameters of decomposition processes of complexes.



**Scheme 1.** Atom numbering representation of Schiff base ligand and its coordination mode to metal center.

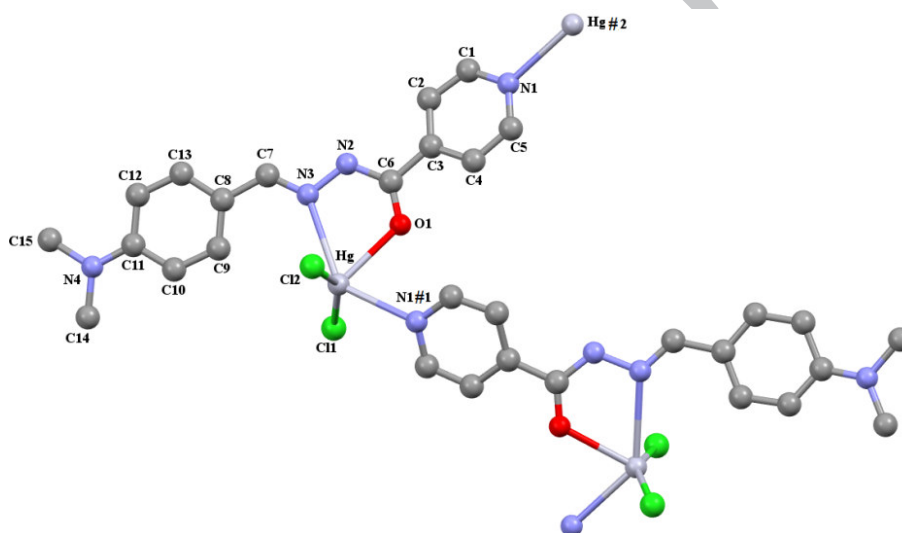


**Fig. 1.** Part of crystal structure of  $[\text{Hg}(\mu\text{-L})\text{Cl}_2]_n$  (**1**). Hydrogen atoms are omitted for clarity. (Symmetry transformations used to generate equivalent atoms: #1:  $-x+1, y+1/2, -z+1/2$  and #2:  $-x+1, y-1/2, -z+1/2$ .)

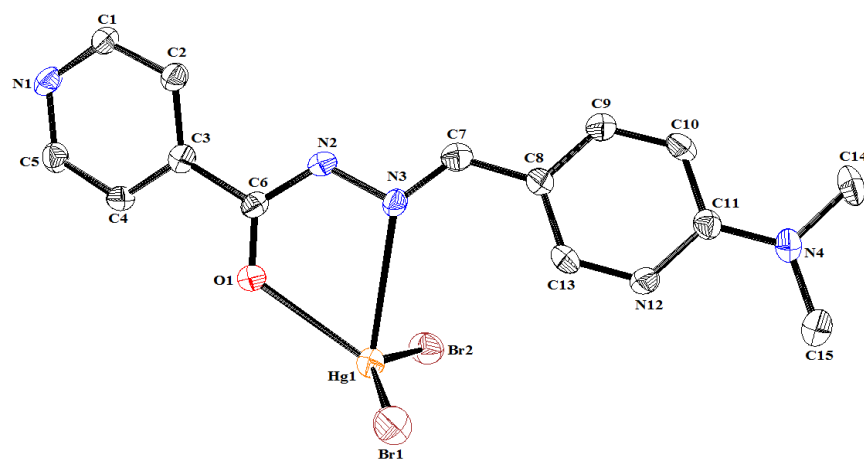


Fig. 2. Asymmetric unit of  $[\text{Hg}(\mu\text{-L})\text{Br}_2]_n$  (**2**), hydrogen atoms are omitted for clarity.

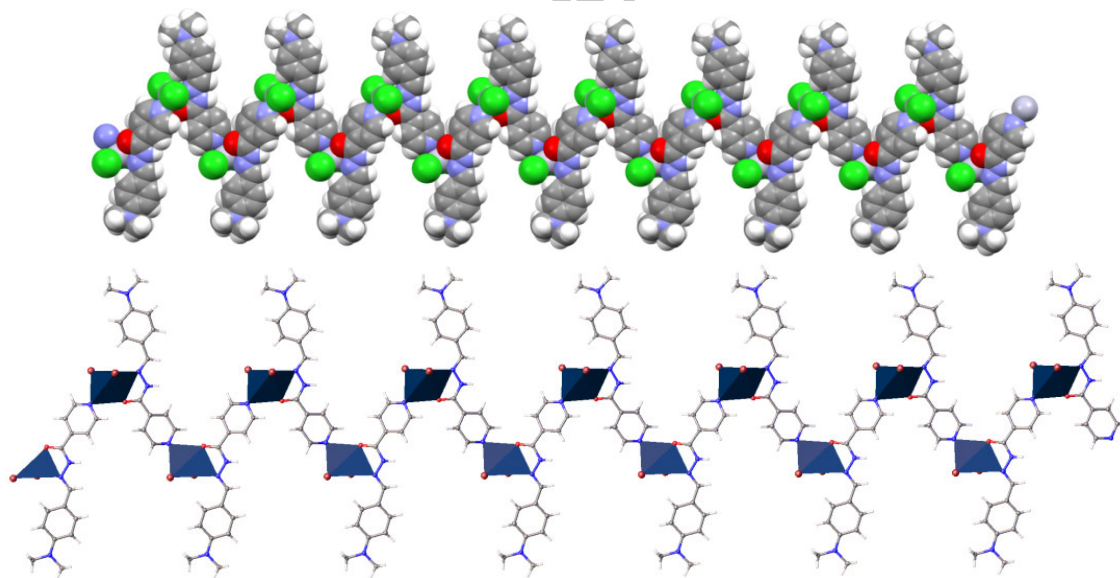


Fig. 3. Polymeric 1D zigzag chain in [top]  $[\text{Hg}(\mu\text{-L})\text{Cl}_2]_n$  (**1**) and [bottom]  $[\text{Hg}(\mu\text{-L})\text{Br}_2]_n$  (**2**).

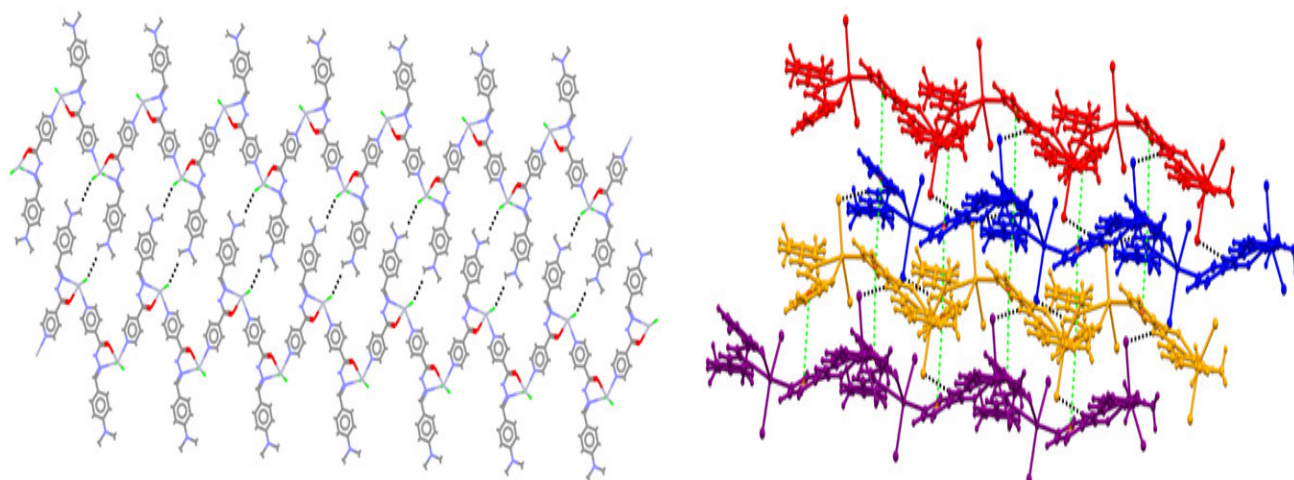


Fig. 4. [left] View of 2D network induced by C-H $\cdots$ Cl interactions and [right] embraced chains by  $\pi\cdots\pi$  stacking and N-H $\cdots$ Cl interactions (green dotted lines:  $\pi\cdots\pi$  stacking and black dotted lines: N-H $\cdots$ Cl interactions) in crystal packing of **1**.

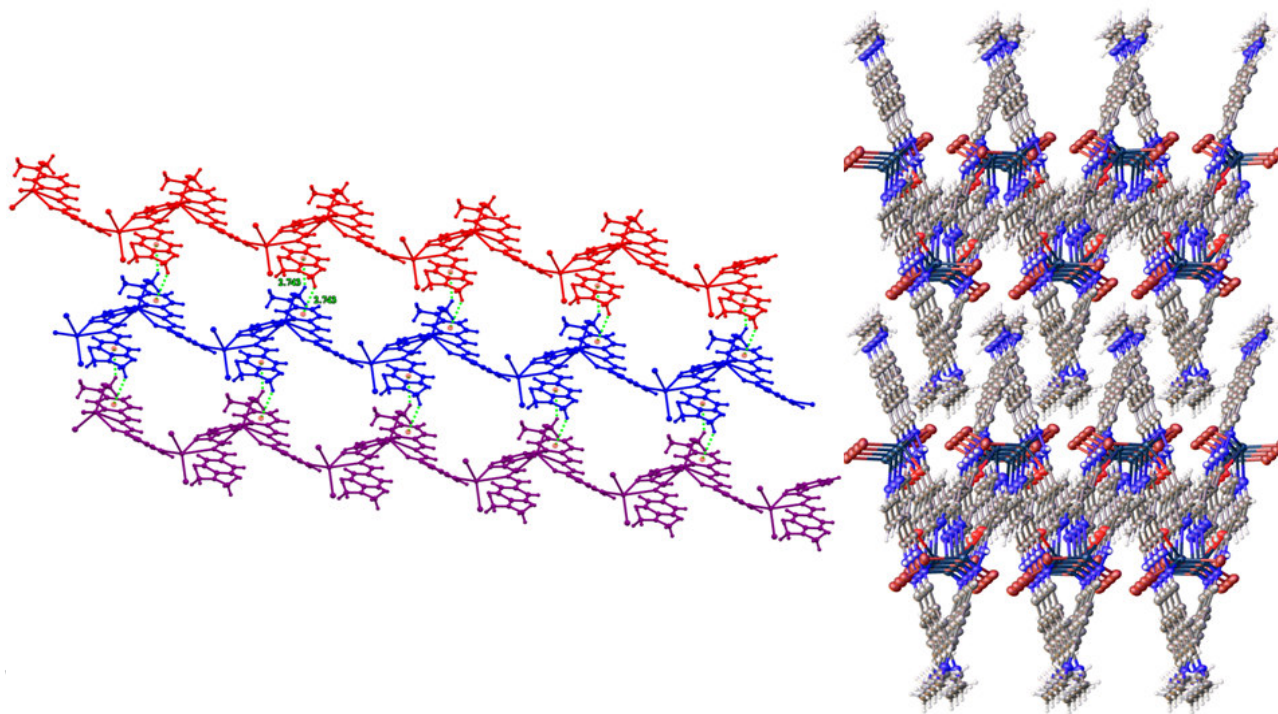


Fig. 5. [left] View of 2D network induced by C-H $\cdots\pi$  interactions and [right] View of 3D supramolecular network induced by intermolecular interactions in **2**.

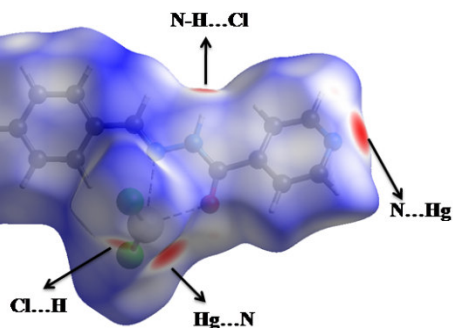


Fig. 6. The Hirshfeld surface of  $[\text{Hg}(\mu\text{-L})\text{Cl}_2]_n$  (1) mapped over  $d_{\text{norm}}$ .

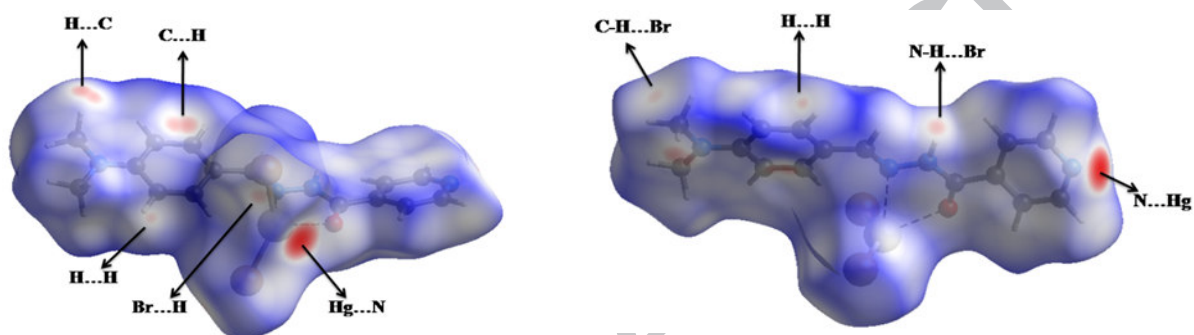


Fig. 7. The Hirshfeld surface of  $[\text{Hg}(\mu\text{-L})\text{Br}_2]_n$  (2) mapped over  $d_{\text{norm}}$  from two different views.

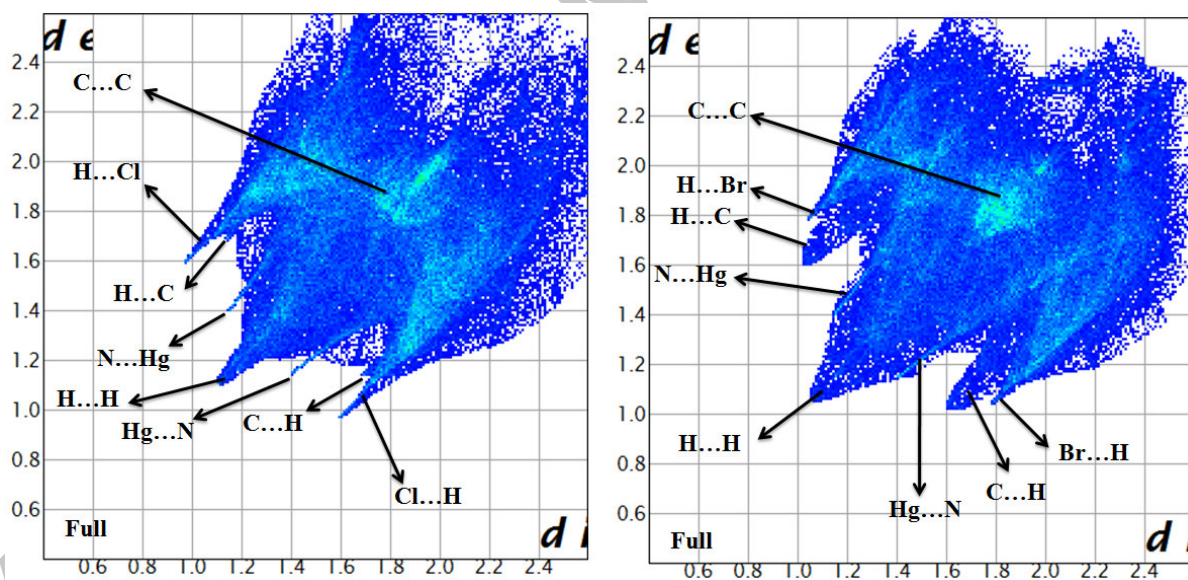
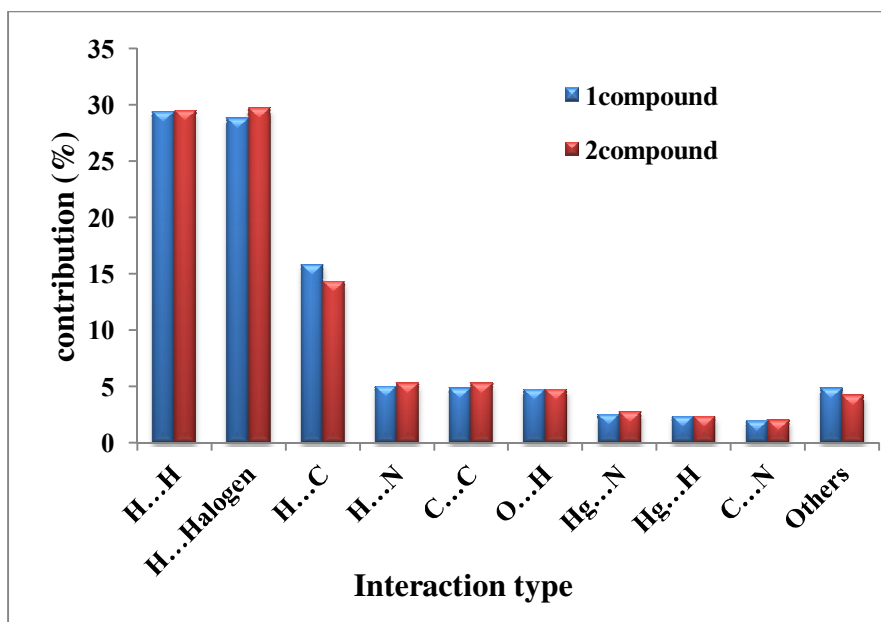
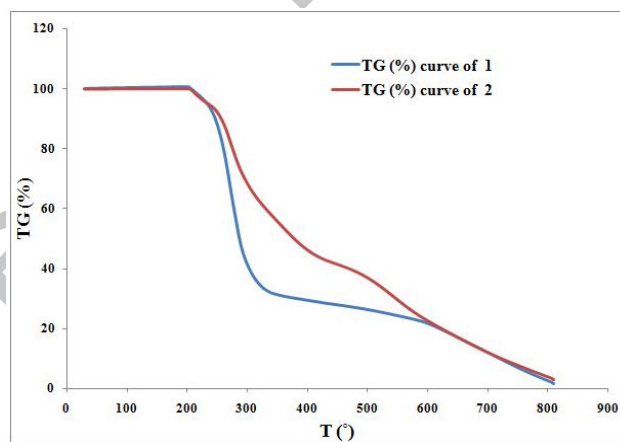


Fig. 8. 2D fingerprint plots of [left]  $[\text{Hg}(\mu\text{-L})\text{Cl}_2]_n$  (1) and [right]  $[\text{Hg}(\mu\text{-L})\text{Br}_2]_n$  (2).



**Fig. 9.** Relative contributions to the Hirshfeld surface area for the various intermolecular contacts in two complexes.



**Fig. 10.** The TG diagrams of both Hg(II) coordination polymers.

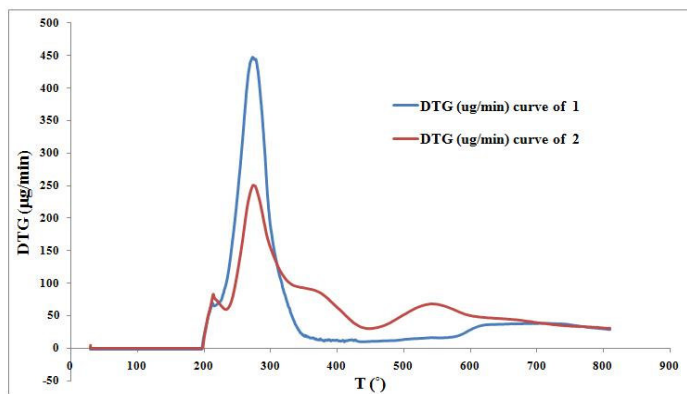


**Fig. 11.** The DTG diagrams of both Hg(II) coordination polymers.

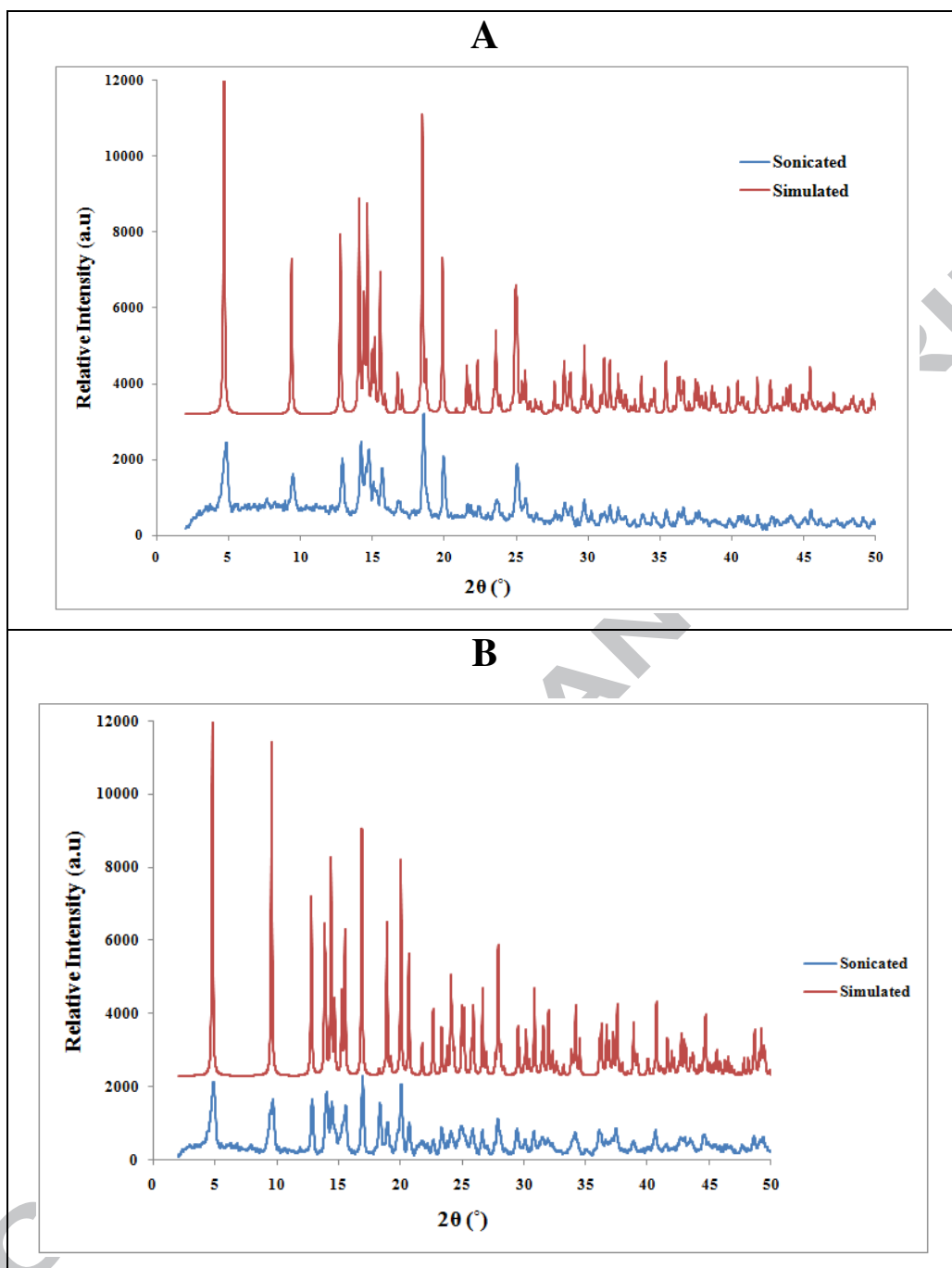


**Fig. 12.** XRD patterns of simulated pattern based on single crystal data and nanostructure prepared by sonochemical process of [A]  $[\text{Hg}(\mu\text{-L})\text{Cl}_2]_n$  (1) and [B]  $[\text{Hg}(\mu\text{-L})\text{Br}_2]_n$  (2).

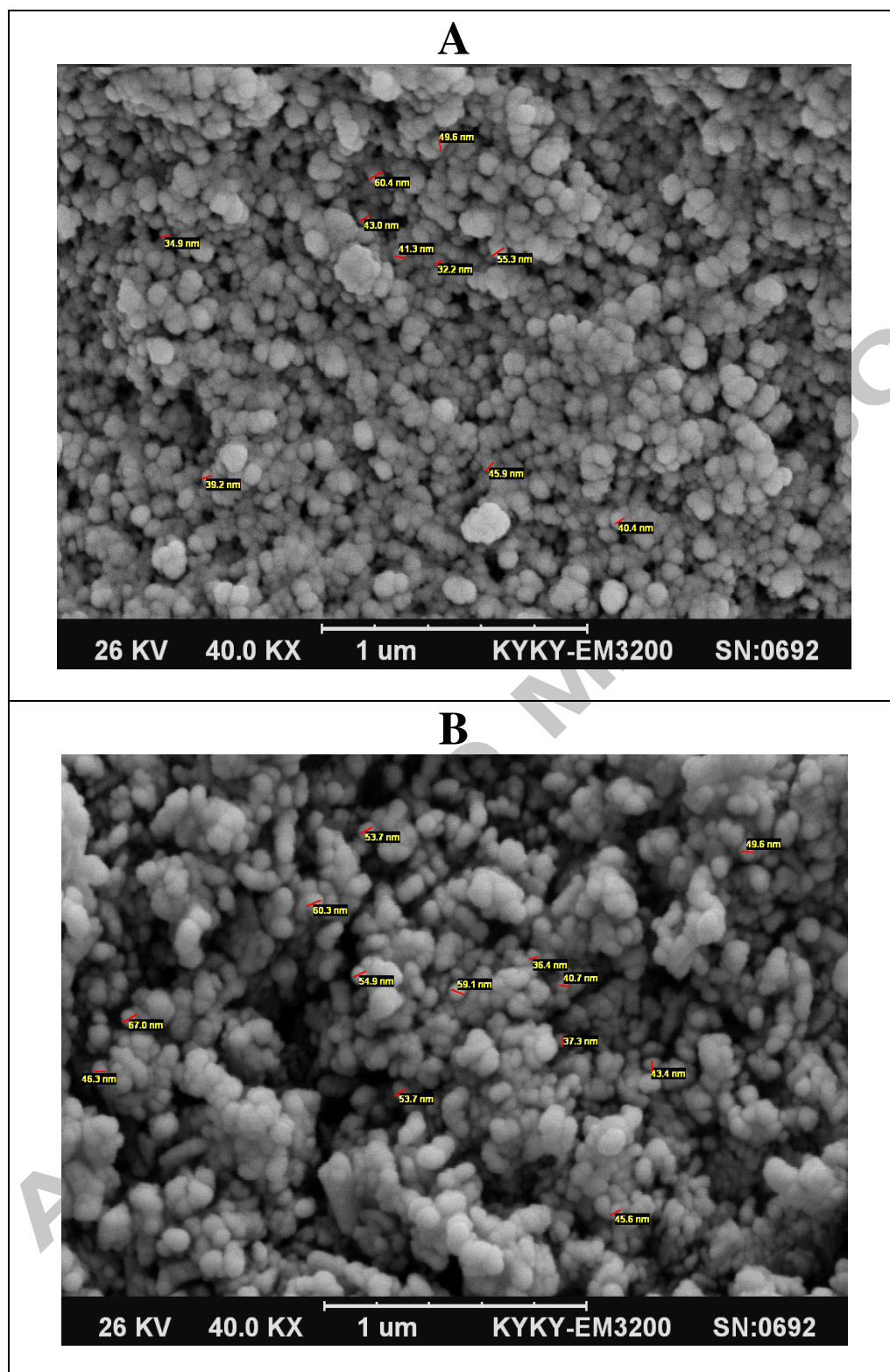


**Fig. 13.** SEM images of coordination polymers **1** (A) and **2** (B) prepared by sonochemical process.

**Table 1**Crystal data and structure refinement for [Hg( $\mu$ -L)Cl<sub>2</sub>]<sub>n</sub> (1), and [Hg( $\mu$ -L)Br<sub>2</sub>]<sub>n</sub> (2)

Compound	(1)	(2)
Empirical formula	C <sub>15</sub> H <sub>16</sub> C <sub>12</sub> HgN <sub>4</sub> O	C <sub>15</sub> H <sub>16</sub> Br <sub>2</sub> HgN <sub>4</sub> O
Formula weight (g/mol)	539.81	628.73
Temperature (K)	296(2)	296(2)
Wavelength (Å)	0.71073	0.71073
Crystal system	Orthorhombic	Orthorhombic
Space group	Pbca	Aba2
Unit cell dimensions	<i>a</i> = 7.4365(16) Å	<i>a</i> = 7.4556(2) Å
	<i>b</i> = 12.437(3) Å	<i>b</i> = 36.8955(11) Å
	<i>c</i> = 37.674(8) Å	<i>c</i> = 12.7559(4) Å
Volume (Å <sup>3</sup> )	3484.4(13)	3508.87(18)
Z	8	8
Calculated density (Mg/m <sup>3</sup> )	2.058	2.380
Absorption coefficient (mm <sup>-1</sup> )	9.149	13.336
<i>F</i> (000)	2048	2336
Crystal size (mm)	0.108 x 0.059 x 0.027	0.146 x 0.077 x 0.023
Theta range for data collection (°)	2.162 to 20.823	3.194 to 27.494
Index ranges	-7 ≤ <i>h</i> ≤ 7, -12 ≤ <i>k</i> ≤ 12, -37 ≤ <i>l</i> ≤ 37	-9 ≤ <i>h</i> ≤ 9, -47 ≤ <i>k</i> ≤ 47, -16 ≤ <i>l</i> ≤ 16
Reflections collected	23554	20527
Independent reflections	1829	3959
<i>R</i> <sub>int</sub>	0.1152	0.0867
Completeness to theta (%)	99.8	99.8
Absorption correction	Semi-empirical from equivalents	Semi-empirical from equivalents
Max. and min. transmission	0.7446 and 0.4782	0.7461 and 0.5523
Refinement method	Full-matrix least-squares on <i>F</i> <sup>2</sup>	Full-matrix least-squares on <i>F</i> <sup>2</sup>
Data/restraints/parameters	1829/0/206	3959/1/211
Goodness-of-fit on <i>F</i> <sup>2</sup>	1.238	1.060
Final <i>R</i> indices [ <i>I</i> > 2σ( <i>I</i> )]	<i>R</i> <sub>1</sub> = 0.0475, <i>wR</i> <sub>2</sub> = 0.1154	<i>R</i> <sub>1</sub> = 0.0358, <i>wR</i> <sub>2</sub> = 0.0785
<i>R</i> indices (all data)	<i>R</i> <sub>1</sub> = 0.0597, <i>wR</i> <sub>2</sub> = 0.1207	<i>R</i> <sub>1</sub> = 0.0426, <i>wR</i> <sub>2</sub> = 0.0801
Largest diff. peak and hole (e.Å <sup>-3</sup> )	1.429 and -0.971	1.863 and -1.769

**Table 2**Bond lengths (Å) and angles (°) for [Hg( $\mu$ -L)Cl<sub>2</sub>]<sub>n</sub> (1) and [Hg( $\mu$ -L)Br<sub>2</sub>]<sub>n</sub> (2)

(1)		(2)	
Bond length (Å)		Bond length (Å)	
Hg–N1 <sup>#1</sup>	2.545(11)	Hg1–N1 <sup>#2</sup>	2.550(8)
Hg–N3	2.800(1)	Hg1–N3	2.760(8)
Hg–O1	2.466(10)	Hg1–O1	2.455(7)
Hg–Cl1	2.339(5)	Hg1–Br1	2.4661(13)
Hg–Cl2	2.369(4)	Hg1–Br2	2.4733(13)
Bond angle (°)		Bond angle (°)	
N1 <sup>#1</sup> –Hg–O1	75.9(4)	N1 <sup>#2</sup> –Hg–O1	78.2(3)
N1 <sup>#1</sup> –Hg–N3	137.16(3)	N1 <sup>#2</sup> –Hg–N3	140.03(2)
N1 <sup>#1</sup> –Hg–Cl1	96.3(3)	N1 <sup>#2</sup> –Hg–Br1	94.7(2)
N1 <sup>#1</sup> –Hg–Cl2	92.9(3)	N1 <sup>#2</sup> –Hg–Br2	97.11(18)
N3–Hg–O1	62.16(4)	N3–Hg–O1	62.29(2)
N3–Hg–Cl1	99.40(3)	N3–Hg–Br1	100.47(2)
N3–Hg–Cl2	91.62(3)	N3–Hg–Br2	91.75(2)
O1–Hg–Cl1	100.6(3)	O1–Hg–Br1	104.5(2)
O1–Hg–Cl2	107.5(3)	O1–Hg–Br2	111.0(2)
Cl1–Hg–Cl2	151.76(16)	Br1–Hg–Br2	144.23(4)

Symmetry transformations used to generate equivalent atoms:

#1 -x+1, y+1/2, -z+1/2

#2 -x+1, -y+1/2, z-1/2

**Table 3**Intermolecular interactions in crystal packing of [Hg( $\mu$ -L)Cl<sub>2</sub>]<sub>n</sub> (**1**) and [Hg( $\mu$ -L)Br<sub>2</sub>]<sub>n</sub> (**2**)

Interaction	D-H...A	D-H (Å)	H...A (Å)	D...A (Å)	A...H-D (°)	Symmetry operation
<b>(1)</b>						
N-H...Cl	N2-H2A...Cl2	0.860	2.703	3.537	164	1-x,1-y,1-z
C-H...Cl	C14-H14C...Cl1	0.960	2.875	3.638	137	1/2-x,1/2+y,z
<b>(2)</b>						
N-H...Br	N2-H2A...Br2	0.859	2.971	3.791	161	1/2-x,y,-1/2+z
C-H...Br	C5-H5...Br2	0.930	3.039	3.781	138	-1/2+x,1/2-y,z
C-H... $\pi$	C14-H14C...Cg2	0.961	2.743	3.558	143	-x,1-y,z

Ring code: Cg2: C8, C9, C10, C11, C12, C13.

**Table 4**

Thermal analysis data including temperature range, mass loss and thermodynamic activation parameters of decomposition processes of complexes.

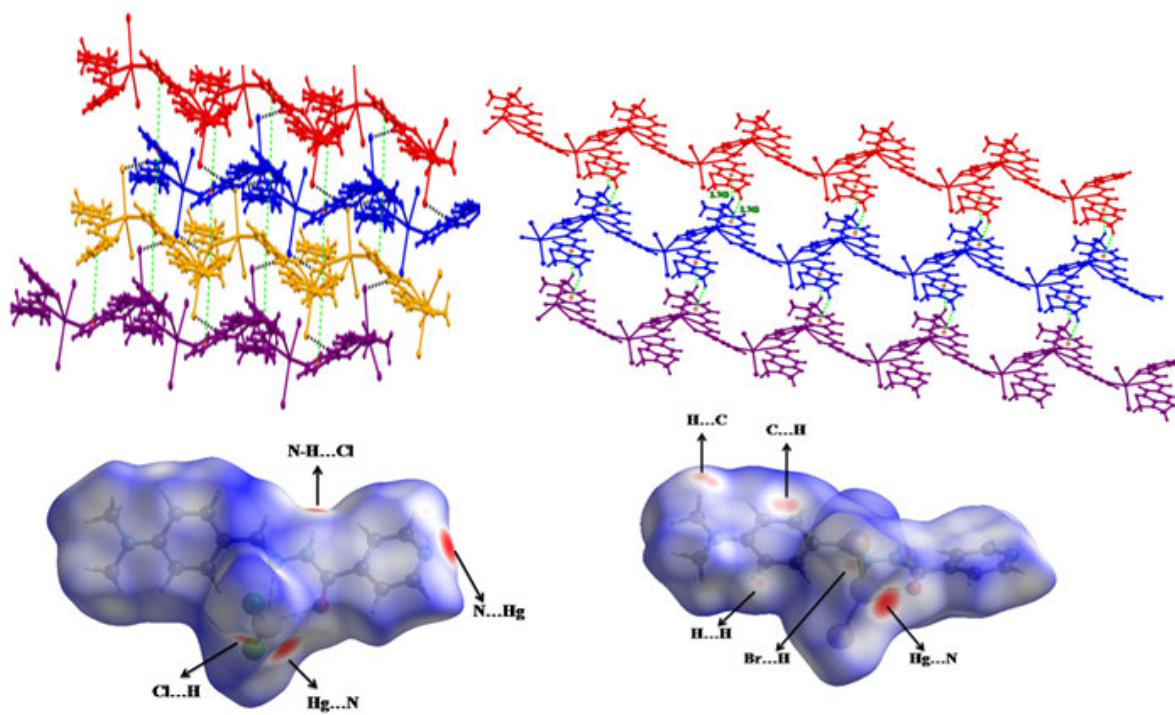
Compound	Temperature	Mass loss (%)	Proposed segment	E* (kJ.mol <sup>-1</sup> )	$\Delta S^*$ (kJ.mol <sup>-1</sup> )	$\Delta H^*$ (kJ.mol <sup>-1</sup> )	$\Delta G^*$ (kJ.mol <sup>-1</sup> )
	step(°C)	exp. (cald)					
[Hg( $\mu$ -L)Cl <sub>2</sub> ] <sub>n</sub>	202-222	2.55(2.77)	CH <sub>3</sub>	588.58	9.23×10 <sup>2</sup>	584.55	1.38×10 <sup>2</sup>
	222-395	61.46(60.00)	C <sub>14</sub> H <sub>13</sub> Cl <sub>2</sub> N <sub>4</sub> O	116.93	-8.48×10 <sup>1</sup>	112.41	1.59×10 <sup>2</sup>
	395-800	35.99(37.22)	Hg	158.37	-1.12×10 <sup>3</sup>	151.06	1.14×10 <sup>3</sup>
[Hg( $\mu$ -L)Br <sub>2</sub> ] <sub>n</sub>	196-223	3.29(2.38)	CH <sub>3</sub>	405.34	5.44×10 <sup>2</sup>	401.31	1.37×10 <sup>2</sup>
	228-300	30.62(31.63)	C <sub>13</sub> H <sub>15</sub> N <sub>2</sub>	109.33	-9.95×10 <sup>1</sup>	104.79	1.59×10 <sup>2</sup>
	320-403	22.66(21.93)	CH <sub>2</sub> BrN <sub>2</sub> O	39.90	-2.39×10 <sup>2</sup>	34.62	1.86×10 <sup>2</sup>
	403-800	43.61(44.51)	HgBr	37.87	-4.01×10 <sup>2</sup>	31.19	3.54×10 <sup>2</sup>
				-			

**Graphical abstract (Synopsis)**

Two new 1D zigzag coordination polymers;  $[\text{Hg}(\mu\text{-L})\text{Cl}_2]_n$  (**1**) and  $[\text{Hg}(\mu\text{-L})\text{Br}_2]_n$  (**2**) were synthesized and identified by single crystal X-ray diffraction. The ligand (L) acts as  $\text{N}_2\text{O}$ -donor. The 1D zigzag chain is stabilized as 3D supramolecular network by intermolecular interactions of  $\pi\cdots\pi$  stacking and  $\text{X-H}\cdots\text{Cl}$  ( $\text{X}=\text{N}$  and  $\text{C}$ ) in **1** and  $\text{C-H}\cdots\pi$ ,  $\pi\cdots\pi$  stacking and  $\text{X-H}\cdots\text{Br}$  ( $\text{X}=\text{N}$  and  $\text{C}$ ) in **2**. Hirshfeld surface analysis and 2D fingerprint plots of asymmetric units of two complexes indicated differences and similarities between crystal packing of compounds. Nanostructure forms of the titled coordination polymers have been also synthesized.

ACCEPTED MANUSCRIPT

Graphical abstract:



ACCEPTED

**Highlights:**

- ▶ Two new 1D zigzag mercury(II) coordination polymers were synthesized.
- ▶ Hg(II) ion is surrounded by three nitrogen atoms of Schiff base and two halide anions.
- ▶ Hirshfeld surface analysis and 2D fingerprint plots of two complexes were investigated.
- ▶ TG/DTG analyses showed completely decomposition of the complexes during 3-4 steps.
- ▶ Nanostructured forms of coordination polymers were sonochemically synthesized.

ACCEPTED MANUSCRIPT